Structural, Electrical and Infrared Studies of $\mathrm{Ni}_{0.7}\mathrm{Cd}_{0.3}\mathrm{Sm}_x\mathrm{Fe}_{2-x}\mathrm{O}_4$ Ferrite

M. Z. SAID, D. M. HEMEDA, S. Abdel KADER and G. Z. FARAG
Physics Department, Faculty of Science, Tanta University, Tanta-EGYPT
e-mail: dahemeda@yahoo.com

Abstract

A series of samples of the system $\mathrm{Ni}_{0.7}\mathrm{Cd}_{0.3}\mathrm{Sm}_x\mathrm{Fe}_{2-x}\mathrm{O}_4$ ($x = 0$, 0.01, 0.02, 0.03, 0.04, 0.05 and 0.06) were prepared by the usual ceramic technique. X-ray diffraction, infrared spectroscopy (IR) and electrical properties were studied. The X-ray diffraction pattern confirms the presence of spinel phase structure for the sample without Sm content. For the samples with Sm ions, some diffraction peaks appeared which belongs to the orthorhombic phase structure. The main two absorption bands in IR spectra were observed around 600 cm^{-1} (v_1), which was attributed to stretching vibration of tetrahedral groups Fe^{3+}–O^{2-}, and that around 400 cm^{-1} (v_2) was attributed to the octahedral group complex Fe^{3+}–O^{2-}. The DC conductivity was found to increase with increasing temperature and Sm addition, which improved the electrical conduction of the given ferrite.

Key Words: Orthoferrites; Spectral studies; DC conductivity; Electrical mobility.

1. Introduction

It is known that the transition metal monoxides such as MnO, CaO, NiO and ferrites such as cobalt ferrite, nickel ferrite and magnesium ferrite behave as semiconductors with low mobility of charge carriers and an exponential dependence of electrical conductivity on temperature. Electrical conduction in these materials has been described by the hopping mechanism. For such process the mobility is strongly dependent on temperature and are found to be proportional to -E_μ/KT, where E_μ is the activation energy of mobility [1]. For $\mathrm{CuAl}_x\mathrm{Fe}_{2-x}\mathrm{O}_4$ the thermoelectric power α is negative and has a constant value over a wide range of temperature and its magnitude increases at higher temperature T [2]. The results indicate that in the range of constant thermoelectric power α, where carrier concentration is constant, the conduction is due to the hopping mechanism. In the range where α increases with temperature, conduction is due to hopping and impurities, which arises from the loss of oxygen during sintering process, and form cations which act as acceptors. The soluble additives in Ni ferrite are Na, Be, Mg, Al, Ga, In, Se and Cr [3]. In Ni ferrite several additives form other phases, in addition to the spinel phase, as Ca, Tl, Nb and Tb. Thermoelectric power of $\mathrm{NiAl}_x\mathrm{Fe}_{2-4}\mathrm{O}_4$ is negative and for $\mathrm{NiAlFeO}_4$ α is positive [4]. The Ni ions favor octahedral site and the conduction mechanism is p-type due to hole transfer from Ni^{3+} to Ni^{2+} $\mathrm{Ni}^{2+} + h \rightarrow \mathrm{Ni}^{3+}$.

In the range where thermoelectric power is dependent on temperature the carrier concentration is constant and the conduction proceeds via hopping mechanism. The constancy of α with T indicates that the number of charge carrier is constant and independent on temperature. This may happen only when charge carriers are localized in the lattice.

It was found that all rare-earth ions favor the occurrence of second phase, resulting in an increase of the electrical resistivity and bulk density. The electronic valence of the rare-earth ions is most important for compound formation. In general, rare-earth ions are most stable when they are trivalent. Only Gd, Er and Lu can be trivalent cations, where Ce and Tb are both trivalent and tetravalent while Sm, Dy are divalent and trivalent [5]. Owing to their large radius compared to that of Fe^{3+} ions, the lattice will be distorted, generating internal stress and increasing the lattice constant. For the composition with orthorhombic second phase, the lattice constant is slightly smaller than unsubstituted ferrite and will decrease with the increase of rare-earth ion radius which suggests the existence of solubility limit for rare-earth ions [6].

The Curie temperature T_c increases with Fe content, but shifts to a lower value as Al content increases in the composition $CuFe_{2-x}Al_xO_4$ [7]. These results are due to the decrease of magnetic Fe^{3+} ions in octahedral sites as nonmagnetic Al^{3+} ions replace them and affect the magnetic order. T_c decreases as Co ion substitution increases in place of Ni in the composition $Co_xNi_{5-x/3}Sb_{1/3}FeO_4$ [8]. In the ferrite system $Ni_xMg_{1-x}Fe_2O_4 T_c$ increases with Ni ion content [9].

Polycrystalline Ni ferrite has been used in many electronic devices because of their high permeability in radio frequency region, high electrical resistivity, high Curie temperature, environmental stability and low price. In the present paper we have investigated the influence of rare-earth Samarium (Sm) ions substituted for iron ions in Ni ferrite on electrical conductivity, thermoelectric power, carrier mobility and Curie temperature.

It is known that the rare-earth oxides are good electrical insulators and have resistivity at room temperature greater than 10^8 Ohm·cm [10]. By introducing a relatively small amount of R_2O_3 instead of Fe_2O_3, a modification of both the structure and the transport properties can be obtained [11].

2.   Experiment

Polycrystalline samples of mixed ferrites $Ni_{0.7}Cd_{0.3}Sm_xFe_{2-x}O_4$ ($x = 0$, 0.01, 0.02, 0.03, 0.04, 0.05 and 0.06) were prepared by a standard ceramic method and sintered at 1200 ^{o}C for 2 h [12]. The X-ray diffraction pattern for each sample was recorded using a Shimadzu model XD-3 X-ray diffractometer. The powder specimens were exposed to CuKα radiation. To record IR spectra, powders were mixed with KBr in the ratio 1:200 by weight to ensure uniform dispersion in the KBr pellet. The mixed powder was then pressed in a cylindrical die to obtain clean discs. The IR spectra in the range of 1000–200 cm^{-1} were recorded at room temperature by using Perkin Elmer model 1430 IR spectrometer. The samples were polished to have uniform parallel surfaces and contacts on the surfaces were made by silver paste. Using a Keithley model 610C electrometer, the DC conductivity for the samples at the temperature range 300–600 K was measured. The samples were inserted between two electrodes inside a cell supported by a furnace. The temperature was measured with a Keithley 871 digital thermometer (using a K type thermocouple) to an accuracy of ±0.1 ^{o}C. The thermo-EMF was measured with a NiCr–Ni thermocouple. Details of the apparatus used are given elsewhere [13].

3.   Results and Discussion

3.1.   X-ray analysis

The x-ray diffraction patterns of the system $Ni_{0.7}Cd_{0.3}Sm_xFe_{2-x}$ O_4 with $x = 0$, 0.01, 0.02, 0.04, 0.05 and 0.06 are shown in Figure 1. The patterns confirm the presence of spinel phase structure for the sample without Sm content. For the samples with Sm ions, some diffraction peaks (such as 020, 110, 112, 113 and 301) appeared which belong to the orthorhombic phase structure. This new phase was formed beside the spinel phase. Also noticed is the change in intensities of some peaks under the effect of Sm substitution. The peaks belong to the orthorhombic phase are given in Table 1.
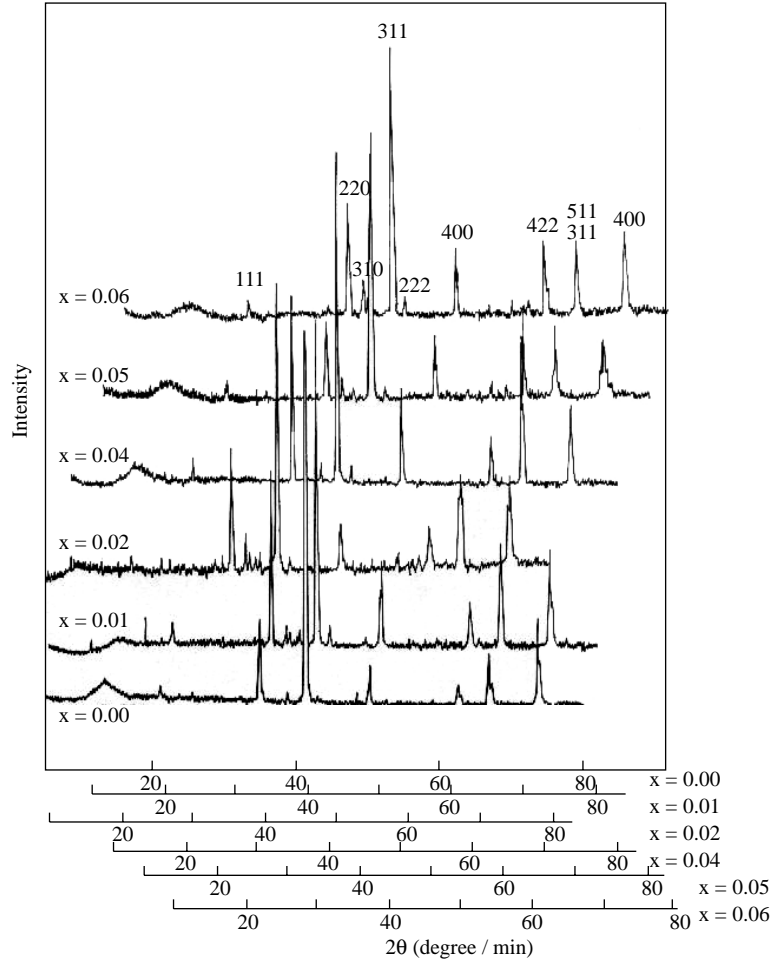
Figure 1. X-ray diffractograms for the different compositions.

Table 1

x = 0.0 1		x = 0.02		x = 0.04		x = 0.05		x = 0.06	
d	hk1	d	hk1	d	Hk1	d	Hk1	d	hk1
				3.8910	110				
2.7082	112	2.6947	112	2.8210	020	2.8210	020	2.8060	020
2.1020	113	2.10226	113	2.722	112	2.6947	112	2.110	113
1.7254	114	1.72047	114	1.7254	213	1.5354	213	1.727	213
				1.708	301				
1.6260	311	1.62603	311	1.626	311	1.6217	311		

The lattice parameter of the spinel phase is given from equation $a = d\sqrt{h^2 + k^2 + 1^2}$ and that for orthorhombic phase is given by

$$d_{h\,k\,l}^2 = \left[\frac{h^2}{a^2} + \frac{k^2}{b^2} + \frac{1^2}{c^2} \right]^{-1}, \tag{1}$$

where h, k, l are the indices of the aforementioned planes. The lattice parameter for the spinel phase is nearly constant, and is varied 8.44–8.47 Å due to the change of Sm content from $x = 0$ to 0.06. As the Sm

ions have radius = 0.1 nm and substitute for Fe^{3+}, which have radius 0.064 nm, the lattice parameter must increase with increasing Sm content. This suggests the second phase orthorhombic phase exert a compression on the spinel phase and prevents its expansion. From the correlation between lattice parameter and ionic radius we can calculate the lattice parameter theoretically from the equation [14]

$$a_{th} = \frac{8}{3\sqrt{3}} \left[(r_A + R_\circ) + \sqrt{3}(r_B + R_\circ) \right] \tag{2}$$

where $R_\circ$ is the radius of the oxygen ions (0.132 nm), and r_A and r_B are the ionic radii of tetrahedral and octahedral sites, respectively. The cation distribution can be suggested as to make a confirmation between a_{th} and a_{exp}. The proposed cation distribution is given in Table 2. As shown in Figure 2, a_{th} is slightly greater than a_{exp}, which may be due to the presence of some ferrous ion (Fe^{2+}) at octahedral sites with larger radius than Fe^{3+}. The radius of tetrahedral r_A is constant while r_B increases with Sm content. This is because the Sm ions has larger radius (0.1 nm) than that of Fe^{3+} and located at octahedral sites.
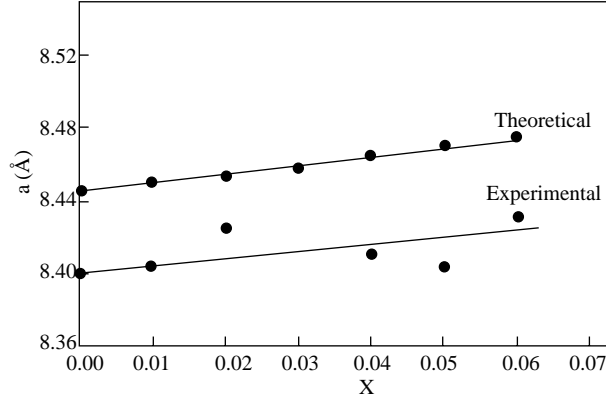
Figure 2. The theoretical and experimental lattice parameters as a function of Sm content x.

Table 2

Composition	a_{th}	a_{exp}	u
$\left[Fe^{3+}_{0.7}Cd^{2+}_{0.3}\right]$ (Ni$_{0.7}$ Fe$_{1.3}$)	8.444	8.443	0.3908
$\left[Fe^{3+}_{0.7}Cd^{2+}_{0.3}\right]$ (Ni$_{0.7}$ S m$_{0.01}$ Fe$_{1.29}$)	8.448	8.406	0.391
$\left[Fe^{3+}_{0.7}Cd^{2+}_{0.3}\right]$ (Ni$_{0.7}$ S m$_{0.02}$ Fe$_{1.28}$)	8.453	8.423	0.391
$\left[Fe^{3+}_{0.7}Cd^{2+}_{0.3}\right]$ (Ni$_{0.7}$ S m$_{0.04}$ Fe$_{1.26}$)	8.462	8.41	0.3913
$\left[Fe^{3+}_{0.7}Cd^{2+}_{0.3}\right]$ (Ni$_{0.7}$ S m$_{0.05}$ Fe$_{1.25}$)	8.467	8.423	0.3914
$\left[Fe^{3+}_{0.7}Cd^{2+}_{0.3}\right]$ (Ni$_{0.7}$ S m$_{0.06}$ Fe$_{1.24}$)	8.471	8.468	0.3909

The oxygen positional parameter u is given by the equation [15]

$$u = \left[(r_A + R_\circ)\frac{1}{\sqrt{3}\,a} + \frac{1}{4} \right], \tag{3}$$

and the calculated values are given in Table 2. Values of u depends on preparation condition, chemical compositions and heating procedure [16]. It has value equal to 0.375 for spinel structure [17]. For our composition, u is greater than this value, which indicates the presence of some deviation from ideal case. Values of u increase with Sm content due to the formation of the orthorhombic phase [18, 19]. The lattice parameters of the second phase (orthorhombic phase) are given in Table 3.

Table 3

x	a	b	c	$V(\mathrm{A}^0)^3$	D_{xs} g/cm^3	D_{xo} g/cm^3
0.01	5.231	5.991	7.456	233.650	5.47	5.38
0.02	5.185	5.806	7.516	226.273	5.66	5.55
0.04	5.373	5.462	7.664	224.918	5.77	5.53
0.05	5.2826	5.5556	7.5882	222.673	5.83	5.82
0.06	5.324	5.612	7.557	225.558	5.80	5.77

The unit cell volume of orthorhombic phase decreases with increasing Sm content due to lattice distortion, which increases with Sm content. The density of the samples was calculated using the spinel phase D_{xs} and orthorhombic phase D_{xo}. The equation $D_{xs} = 8M/Na^3$, where a is the lattice parameter of spinel phase and the equation $D_{xo} = 3M/NV$ for the orthorhombic phase, which is an empirical equation and gives good results compared with the density of the sample calculated from the spinel phase equation.

The densities of the samples are given in Table 3. The theoretical densities of the sample were given from X-ray data. The bulk density and the porosity are shown in Figure 4 as a function of Sm content. The porosity is given by the relation $P = 1-(D/D_x)$. The density of the samples increases with Sm content due to the function of the second phase, which compress the lattice and increase the density. The porosity decreases with increasing Sm content, which means that the addition of Sm accelerates the densification process during sintering.
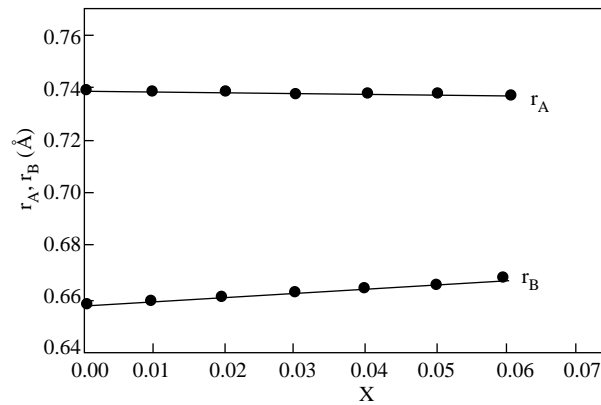

Figure 3. The radius of tetrahedral sites r_A and octahedral sites r_B as a function of Sm content x.
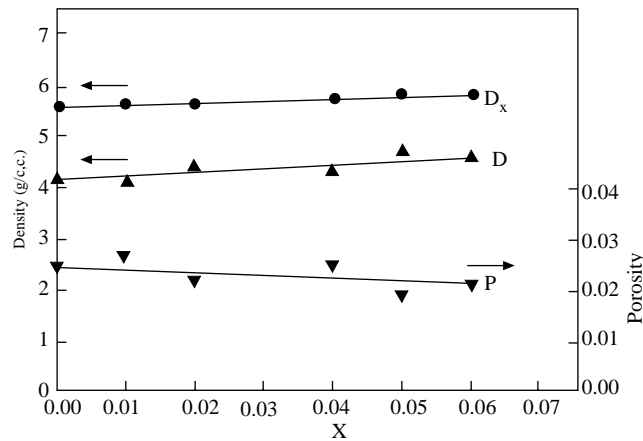

Figure 4. The density and porosity as a function of Sm content x.

3.2. IR spectral analyses

The IR absorption spectra of the samples in the range 1000–200 cm^{-1} are given in Figure 5. For ferrites, two assigned absorption bands appeared around 600 cm^{-1}: ν_1, which was attributed to stretching vibration of tetrahedral groups Fe^{3+}–O^{2-} and that around 400 cm^{-1}, and ν_2, which was attributed to the octahedral groups complex Fe^{3+}–O^{2-}. In the present spectra, band ν_1 appears near 560 cm^{-1} and shifts to lower frequency with Sm^{3+} addition. The second absorption band ν_2 appears near 446 cm^{-1} and also shifts to lower frequencies with Sm addition. The differences in frequencies between ν_1 and ν_2 is due to changes in bond length (Fe^{3+}–O^{2-}) at octahedral and tetrahedral sites [20]. Thus from X-ray analysis it was found Sm ions dissolved in the material and substitute for Fe^{3+} at octahedral sites. No band indicates the vibration of Sm^{3+}–O^{2-} ions due to its small ratio. The IR bands and their intensities for all samples under investigation are given in Table 4. The intensity of IR absorption band is a function of the ionic population [21]. Accordingly, I_A and I_B change with increasing Sm content. The shifts occur in the frequency band ν_1 and ν_2 for each octahedral and tetrahedral sites are due to the perturbation occurring in the Fe^{3+}–O^{2-} band by introducing Sm ions. The IR band width depends on the cation distribution of the material. As shown in X-ray analysis, the cation distribution at tetrahedral sites are the same for all samples. On this assumption we found that the band width for tetrahedral sites is nearly constant for all samples, but that of octahedral sites increase with Sm content, as shown in Figure 6.
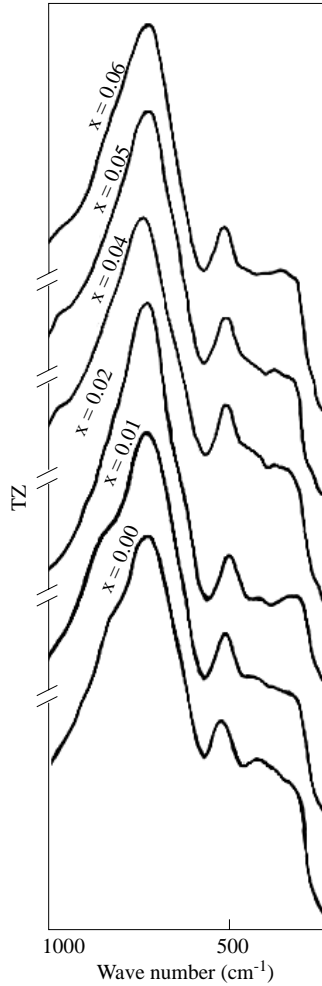
Figure 5. IR spectra of the given compositions.
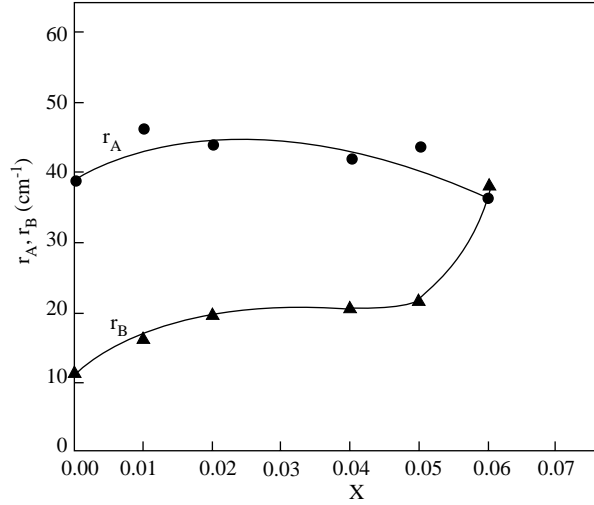
Figure 6. The line width of the IR absorption bands for both A and B sites as a function of Sm content x.

Table 4.

| x	I_A (a.u.)	I_B (a.u.)	v_1 (cm^{-1})	v_2 (cm^{-1})	f_t (dyne/cm)	f_o (dyne/cm)
0	43.2	41.3	560	446	2.327×10^5	1.47×10^5
0.01	37.5	37.8	558	442	2.3109×10^5	1.494×10^5
0.02	24.7	24.1	556	377	2.294×10^5	1.054×10^5
0.04	40.2	-	555	-	2.286×10^5	-
0.05	36.0	33.6	555	377	2.286×10^5	1.054×10^5
0.06	38.0	37.0	553	376	2.269×10^5	1.049×10^5

The force constant for the bond Fe^{3+}–O^{2-} was calculated from the equation $f = 4\pi^2 c^2 v^2 \mu$ [22], where c is the velocity of light, v is the band wave number in cm^{-1} and μ is the reduced mass. The frequency bands v_1 and v_2 shift to lower frequencies indicating that the force constant decreases with increasing Sm content. The force constant for tetrahedral sites f_t and for octahedral sites f_o are given in Table 4. As shown, f_t is greater than f_o, indicating the band frequency associated with tetrahedral sites is higher than for octahedral sites. The intensity ratio is a function of the change in the dipole moment in the material, so the IR gives information about the change in the molecular structure of ferrite due to changes in the bond Fe^{3+}–O^{2-} coming from the introduction of Sm ions.

3.3.   Electrical conductivity

Figure 7 shows the relation between $\log \rho$ and $10^3/T$ for all samples. As shown, the addition of Sm ions decreases electrical resistivity and increases conductivity. The relation has three lines with two breaks. The first region is the region where the conduction is due to extrinsic impurities in the material behaves like a semiconductor and the band theory is applied. The second region (ferromagnetic region) is the hopping conduction region, with a break at certain temperature T_c, called the Neel temperature, and leads to the third region (paramagnetic region). In the case of Ni ferrite, the following reaction are present [23]:

$$Ni^{2+} + Fe^{3+} \xleftrightarrow{h} Ni^{3+} + Fe^{2+}$$
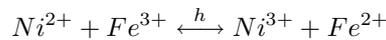
where both Ni^{2+} and Fe^{2+} ions prefer to occupy octahedral sites. So conduction occurs as a result of the electron transfer between Fe^{2+} and Fe^{3+} and hole transfer between Ni^{2+} and Ni^{3+} at octahedral sites.
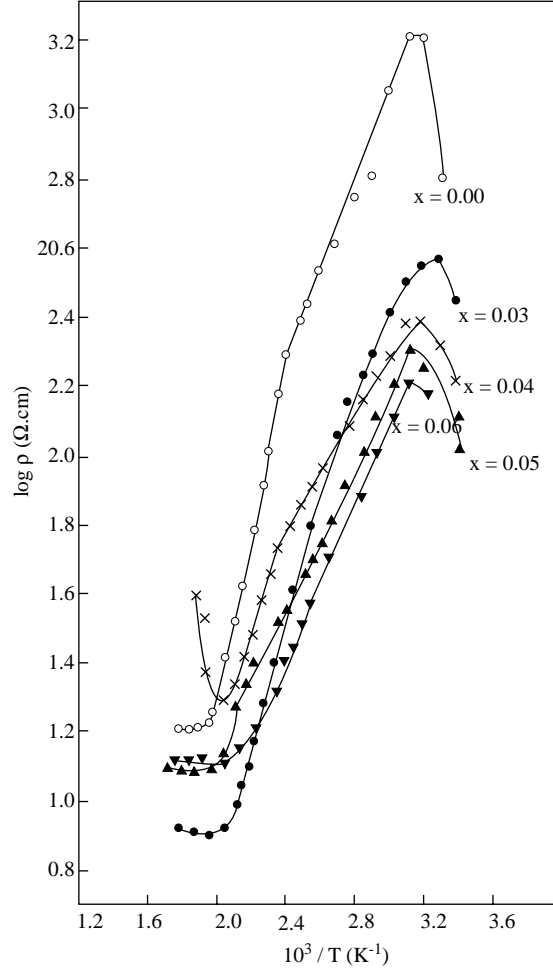
Figure 7. The variation of the resistivity $\log \rho$ versus $10^3/T$ for different samples.

Taking into account the energy level diagram given by Bataut and Delorm [24], where Cd ions lie between Fe^{2+} and Ni^{2+} ions, the existence of Cd ions resist the shift of fermi level towards Fe^{2+} ions and therefore requires a relatively high energy to form charge carriers. The Sm^{3+} ions, which substitute for Fe^{3+} at octahedral sites, have energy level which shift the Fe^{3+} energy level towards the Ni^{2+} level and gives rise to the reaction

$$Ni^{2+} + Fe^{3+} \rightarrow Ni^{3+} + Fe^{2+}$$
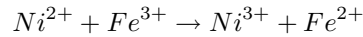
causing the hopping conduction mechanism between Fe^{2+} and Fe^{3+} to increase. The transition temperature shifts to lower temperature with increasing Sm content. The non-magnetic Sm ions replace the paramagnetic Fe^{3+} ion which reduces the total magnetic moment of the material and helps the material to go into Ferro Para transition at lower temperature.

We can conclude that the Sm ions improve the electrical properties of the material for use in many microelectronic applications. Table 5 shows the activation energy for conduction process and the transition temperature T_c.

Therefore, it is expected that the substitution of Fe^{3+} ions by Sm^{3+} ions leads to increase of charge carriers concentration (n) resulting in the increase of the hopping probability between Fe^{2+} and Fe^{3+} ions at octahedral sites This increase of n is due of the presence of two predominant conduction mechanisms: electron hopping between Fe^{2+} and Fe^{3+} ions at octahedral sites, and band conduction [25]. This also leads

to increase of electrical conductivity. It is known that the higher the conductivity the lower the activation energy [26]. Therefore, the substitution of Fe^{3+} by Sm^{3+} ions is followed by a lowering of activation energy.

Table 5

x	E (eV)	T_c (K)
0	0.211	526
0.03	0.155	495
0.04	0.129	476
0.05	0.096	476
0.06	0.08	434

4.   Conclusion

The X-ray diffraction studies show that the Sm addition is not soluble in the spinel phase but instead forms another orthoferrite phase, which exerts pressure on the spinel phase and prevents its expansion due to Sm addition. The lattice parameter did not change with Sm addition, but the oxygen positional parameter values showed a deviation from the ideal spinel case which indicate the presence of some distortion in the unit cell due to Sm addition.

The IR studies show the presence of two assigned absorption bands around 600 cm^{-1} (ν_1) and 400 cm^{-1} (ν_2) which were attributed to the tetrahedral and octahedral group complexes. There was no absorption band due to Sm^{3+}–O^{2-} bond which confirms the X-ray studies that Sm ions do not dissolved in the spinel phase. The variation of the values of the band frequencies, intensity and band width with the addition of Sm ions were attributed to the perturbation occurs in Fe^{3+}–O^{2-} bond due to Sm addition.

The electrical conduction of $Ni_{0.7}Cd_{0.3}Sm_xFe_{2-x}O_4$ was improved its properties by introducing Sm ions in the materials.

References

[1] R. R. Heiks, W. D. Johnson, *J. Chem. Phys.,* **26**, (1957), 582.

[2] M. A. Ahmed, M. A. El-Hiti and M. E. El-Shabasy, *Fizica*, **A3**, (1994), 25.

[3] J. Tasaki, T. Izushi, *J. De Physique*, **38**, (1977), 175.

[4] M. A. Ahmed, M. K. El-Nimr, A. Tawfik, A. M. El-Hassab, *Phys. Stat. Sol. (a),* **123**, (1991), 501.

[5] B. Johanson, *J. Phys. Chem. Solids*, **39**, (1978), 467.

[6] H. Takagi, S. Uchida, H. Eisaki and S. Tanaka, *J. Appl. Phys.*, **63**, (1988), 4009.

[7] E. A. Thuraka Vaskili, T. D. Bakruma, V. Ya Garmash, G.S. Podvalnyul, *Sov. Phys. Powder and Metall. Ceram.*, **23**, (1984).

[8] M. A. El-Hiti, M. K. El-Nimr, M. A. Ahmed, *Phase transition*, **54**, (1995), 137.

[9] M. A. El-Hiti, *Phase transition*, **54**, (1995), 117.

[10] N. Bogoroditzkii, V. V. Pasynkov, R. R. Basili, Yu. M. Volokbinskin, *Soviet Phys. Doklady*, **10**, (1965), 85.

[11] E. Rezlescu, N. Rezlescu, P. D. Popa, L. Relesceu, C. Pasnicu, *Phys. Stat. Sol. (a),* **162**, (1997), 673.

[12] I. M. Hamada, *J. Magn. Magn. Mater.,* **270,** (2004), 318.

[13] A. A. Ghani, M. A. Ahmed, *Proc. Math. Phys. Soc. Egypt*, **12**, (1976).

[14] O. M. Hemeda, M. El Saadawy, M.M.Barakat, *J. Magn. Magn. Mater.,* **219,** (2000), 73.

[15] O. M. Hemeda, M. Z. Said, M. M. Barakat, *J. Magn. Magn. Mater.,* **224**, (2001), 132.

[16] Y. Khan, E. Kneller, *J. Magn. Mater.,* **7**, (1978), 9.

[17] E. J. W. Verwey, E. Z. Heilman, *J. Chem. Phys.,* **15**, (1947), 174.

[18] V. M. Talanov, I. V. Vuzov, *Khim Technol.,* **12,** (1978).

[19] G. I. Ciufarov, Yu. P. Vorobiev, *Fizichoskaya Khimiya Okislov Metallov*, (Izd, Nauka, Moscow, 1981).

[20] O. M. Hemeda, *J. Magn. Magn. Mater*, **281**, (2004), 36.

[21] E. B.Wilson, A. J. Wells, *J. Chem. Phys.,* **14**, (1946), 578.

[22] S. A. Mazen, M. H. Abdallah, B. A. Sobrah, H. A. M. Hashem, *Phys. Stat Sol. A*, **134**, (1992), 263.

[23] L. G. VanVitert, *J. Chem. Phys.,* **23**, (1955), 10.

[24] F. Bertaut, G. Delorm, *C.R. Ac. Sci.*, **239**, (1954), 504.

[25] O. M. Hemeda, M. M. Barakat, D. M. Hemeda, *Turk. J. Phys*, **27**, (2003), 537

[26] O. M. Hemeda, M. M. Barakat, *J. Magn. Magn. Mater*, **223**, (2001), 127.